Int. J. Heat Mass Transfer. Vol. 10, pp. 219–235. Pergamon Press 1967. Printed in Great Britain

FLOW AND HEAT TRANSFER IN THE BOUNDARY LAYER ON A CONTINUOUS MOVING SURFACE

F. K. TSOU,* E. M. SPARROW and R. J. GOLDSTEIN

Heat Transfer Laboratory, Department of Mechanical Engineering, University of Minnesota, Minneapolis, Minnesota

(*Received* 27 *January* 1966 *and in revised form* 30 *May* 1966)

Abstract—A combined analytical and experimental study of the flow and temperature fields in the boundary layer on a continuous moving surface has been carried out. The investigation includes both laminar and turbulent flow conditions. The analytical solutions provide results for the boundary-layer veolcity and temperature distributions and for the surface-friction and heat-transfer coefficients. Measurements of the laminar velocity field are in excellent agreement with the analytical predictions, thereby verifying that a mathematically describable boundary layer on a continuous moving surface is a physically realizable flow. Experimentally determined turbulent velocity profiles are also in very good accord with those of analysis. Similar agreement is found to exist for friction coefficients deduced from the data by application of the Clauser-plot technique. Temperature distribution measurements, carried out for the turbulent boundary layer, show satisfactory correspondence with analysis.

NOMENCLATURE

c_f, local friction coefficient $(\tau_w/\frac{1}{2}\rho U_s^2)$;
$\bar{c}_f$, average friction coefficient $[(D/x)/\frac{1}{2}\rho U_s^2]$;
c_p, specific heat, constant pressure;
D, drag force;
f, dimensionless stream function;
h, local heat-transfer coefficient;
I, definite integral, equation (22);
k, thermal conductivity;
Nu, local Nusselt number, hx/k;
Pr, Prandtl number, $c_p\mu/k$;
Re, Reynolds number, $U_s x/\nu$;
St, Stanton number, $h/\rho c_p U_s$;
q, heat flux/time-area;
T, temperature;
T^+, dimensionless temperature $[(T_w - T)\,\rho c_p\sqrt{(\tau_w/\rho)}/q_w]$;
U_s, surface velocity;
u, streamwise velocity;
u^+, dimensionless velocity $[u/\sqrt{(\tau_w/\rho)}]$;
u_s^+, dimensionless surface velocity $[U_s/\sqrt{(\tau_w/\rho)}]$;
u^{++}, dimensionless velocity $(u_s^+ - u^+)$;
v, transverse velocity;
x, streamwise coordinate;
y, transverse coordinate;
y^+, dimensionless normal coordinate $[y\sqrt{(\tau_w/\rho)}/\nu]$.

Greek symbols

δ, boundary-layer thickness;
ϵ_h, ϵ_m, eddy diffusivities;
η, similarity variable;
θ, dimensionless temperature $[(T - T_\infty)/(T_w - T_\infty)]$;
μ, absolute viscosity;
ν, kinematic viscosity;
ρ, density;
τ, shear stress;
φ, dimensionless temperature $[(T - T_\infty)\sqrt{(Re)}/(q_w x/k)]$.

Subscripts

w, at the surface;
∞, in the ambient fluid.

INTRODUCTION

IN RECENT years consideration has been given

* Present address: Department of Mechanical Engineering, Drexel Institute of Technology, Philadelphia, Pennsylvania 19104.

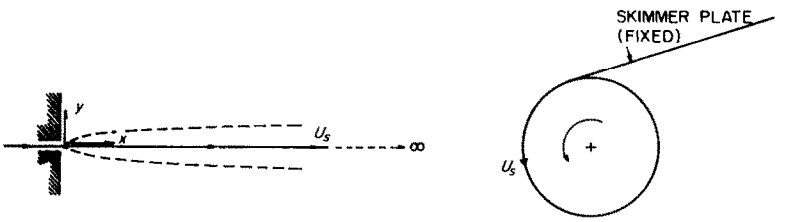

FIG. 1. Schematic representation of the boundary layer on a continuous moving surface.

to a somewhat novel type of flow situation that has been designated as the boundary layer on a continuous moving surface. The essential features of such a flow are illustrated schematically in the left-hand sketch of Fig. 1. An unending plane sheet issues from a slot and moves steadily to the right through an otherwise quiescent fluid environment. Owing to the action of viscosity, the motion of the surface induces a motion in the adjacent fluid. With increasing downstream distance from the slot, the region of flow penetrates deeper and deeper into the environment. Thus, the velocity boundary layer is seen to grow in the direction of motion of the surface. This characteristic is just reversed to that for a semi-infinite flat plate moving through a quiescent environment, wherein the boundary layer grows in the direction opposite to that in which the plate is moving. Interested readers are referred to a series of papers by Sakiadis [1–3] for further background on the boundary layer on a continuous moving surface.

The study to be reported here is a wide-ranging analytical and experimental investigation of the flow and heat-transfer characteristics of the boundary layer on a continuous moving surface. Consideration is given to both laminar and turbulent flows. In the analytical phase, exact solutions are obtained for the laminar velocity and temperature problems, the latter for the two fundamental thermal boundary conditions of uniform wall temperature and uniform wall heat flux. In the case of turbulent flow, the law-of-the-wall model is applied to solve the velocity problem. In turn, the velocity results are employed to solve the temperature problem for the case of uniform wall heat flux. An experimental apparatus was constructed to verify the results of analysis. Measurements of the laminar velocity field demonstrated that the boundary layer on a continuous surface is, in fact, a physically realizable flow. The turbulent velocity field was also investigated by probe measurements, and friction factor results were deduced. Lastly, explorations of the turbulent temperature field were carried out with a thermocouple probe.

The boundary layer on a continuous moving surface was first examined by Sakiadis [1–3]. Approximate and exact solutions for the laminar velocity field were derived. For the turbulent case, an approximate analysis was performed using a one-seventh power velocity profile. If the plane surface is replaced by a cylindrical one (for example, a wire), then the boundary-layer flow is axisymmetric. This case was singled out for study by Koldenhof [4] who was concerned with the movement of fine threads through a liquid. Very recently, in an investigation contemporaneous with the present study, Erickson *et al.* [5] analyzed the laminar heat transfer for the special case in which the surface cools, owing to heat capacity effects, as it moves through the fluid environment.

From the foregoing survey, it is evident that there is a need for definitive experiments as well as for further analysis for the continuous-surface boundary layer.

ANALYSIS

The coordinates appropriate to the boundary-layer analysis are shown in the left-hand diagram of Fig. 1. The velocity components corresponding to the x and y directions are

respectively denoted by u and v. The velocity of the moving surface is denoted by U_s.

Laminar boundary layer

The exact solution for the laminar boundary layer has previously been derived by Sakiadis. His analysis is briefly reviewed and amplified here as a prelude to the heat-transfer problem. The boundary-layer momentum and mass conservation equations may be reduced to a single ordinary differential equation by employing a similarity transformation as follows:

$$\eta = y\sqrt{\left(\frac{U_s}{\nu x}\right)}, \qquad u = U_s f',$$

$$v = \tfrac{1}{2}\sqrt{\left(\frac{\nu U_s}{x}\right)}(\eta f' - f) \quad (1)$$

in which η is the similarity variable and f is a reduced stream function that depends only on η. The prime denotes differentiation with respect to η. The end result of the transformation is

$$f''' + \tfrac{1}{2}ff'' = 0. \quad (2)$$

The foregoing is immediately recognized as the Blasius equation which also describes the laminar flow over a semi-infinite flat plate.

The physical boundary conditions that $u = U_s$ and $v = 0$ at the surface and that $u \to 0$ in the environment become

$$f'(0) = 1, \quad f(0) = 0, \quad f'(\infty) = 0. \quad (3)$$

Compared with the classical Blasius problem, the boundary conditions for $f'(0)$ and $f'(\infty)$ are interchanged. The nonlinearity of equation (2) has precluded the transformation of one problem into the other.

A numerical solution of equations (2) and (3) yields the velocity profile shown as the solid line labeled $f'(\infty) = 0$ in the left-hand portion of Fig. 2. For purposes of comparison, the Blasius velocity profile, represented as $1 - (u/U_\infty)$, is also shown in the figure by a dashed line. It is evident that the profile for the present problem is steeper at the wall and flatter near the edge of the boundary layer. Also appearing in the figure are illustrative solution curves for cases in which $f'(\infty) > 0$. Physically, this corresponds to the case in which the ambient fluid is moving with a velocity U_∞ in the same direction as the surface, wherein $f'(\infty) = U_\infty/U_s$.

The local wall shear stress τ_w may be represented by a dimensionless friction coefficient by employing the following definitions

$$c_f = \frac{\tau_w}{\frac{1}{2}\rho U_s^2}, \qquad Re = \frac{U_s x}{\nu}. \quad (4)$$

In terms of these variables

$$c_f\sqrt{(Re)} = 2f''(0). \quad (4a)$$

For the continuous-surface boundary layer, $c_f\sqrt{(Re)} = 0{\cdot}888$, while the corresponding numerical constant for the Blasius flow is 0·664. Thus, the friction coefficient for the present problem exceeds that for the flat plate.

Consideration may now be given to the heat-transfer problem. Corresponding to the two fundamental boundary conditions of uniform wall temperature (UWT) and uniform heat flux (UHF), it is convenient to respectively define the following dimensionless temperature variables

$$\theta(\eta) = \frac{T - T_\infty}{T_w - T_\infty},$$

$$\varphi(\eta) = \frac{(T - T_\infty)\sqrt{(Re)}}{q_w x/k} \quad (5)$$

in which T_w and T_∞ denote the surface and environment temperatures, and q_w is the wall heat flux. In the first of equations (5), T_w is a constant; while in the second of equations (5), q_w is constant. When the similarity transformation is applied to the boundary-layer energy equation for constant-property, nondissipative laminar flow, there are derived the following governing equations for θ and φ

$$\theta'' + \tfrac{1}{2}Prf\theta' = 0 \qquad \theta(0) = 1, \quad \theta(\infty) = 0 \quad (6)$$

$$\varphi'' - \tfrac{1}{2}Pr(f'\varphi - f\varphi') = 0$$

$$\varphi'(0) = -1, \quad \varphi(\infty) = 0 \quad (7)$$

in which Pr denotes the Prandtl number.

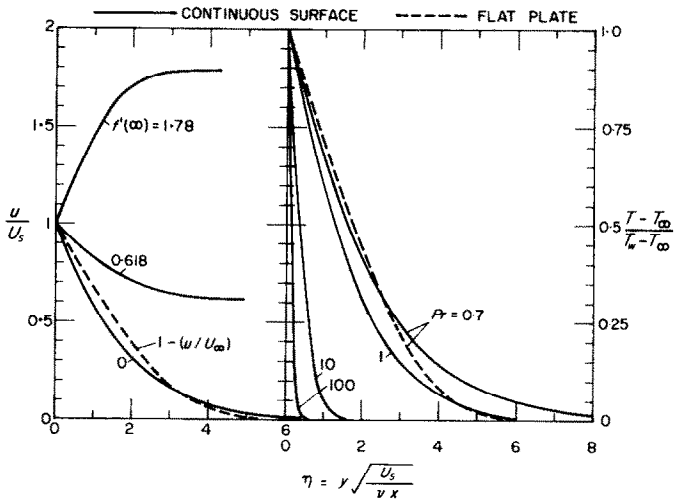

FIG. 2. Velocity and temperature profiles for laminar flow.

The foregoing ordinary differential equations have been solved numerically for $Pr = 0{\cdot}7$, 1, 10 and 100. Boundary-layer temperature profiles for the uniform wall temperature case are presented in the right-hand portion of Fig. 2. These curves show that the thickness of the thermal boundary layer decreases sharply with increasing Prandtl number. Moreover, by comparing the left- and right-hand portions of Fig. 2, it is evident that, as expected, the thermal boundary layer is much thinner than the velocity boundary layer when the Prandtl number is high. For purposes of comparison, the temperature profile for the Blasius problem is shown as a dashed line ($Pr = 0{\cdot}7$). Relative to the Blasius profile, the present temperature distribution is steeper near the wall and flatter near the edge of the boundary layer. The temperature profiles for the uniform heat flux case are similar to those for uniform wall temperature and are omitted in order to conserve space.

The heat-transfer capabilities of the flow may be expressed in terms of a local heat-transfer coefficient h and a local Nusselt number Nu defined as follows

$$h = \frac{q_w}{T_w - T_\infty} \qquad Nu = \frac{hx}{k}. \tag{8}$$

In terms of the variables of the analysis, one finds

$$Nu/\sqrt{(Re)} = \theta'(0)$$

$$\text{and} \qquad Nu/\sqrt{(Re)} = \frac{1}{\varphi(0)} \tag{8a}$$

respectively for uniform wall temperature and uniform wall heat flux. It can be shown that for large Prandtl numbers,* $Nu/\sqrt{(Re)} \sim \sqrt{(Pr)}$. Correspondingly, the results of the numerical solutions have been phrased in terms of $Nu/\sqrt{(RePr)}$ and listed in Table 1.

Inspection of the table reveals that at any given Prandtl number, the heat-transfer coefficient for uniform heat flux exceeds that for uniform wall temperature by 55 to 70 per cent. This qualitative relationship between the coefficients is well established for laminar flows. The asymptotic behavior for high Prandtl numbers is not fully achieved in the Prandtl number range investigated here, although it is clear that the limiting behavior is being approached.

It is of interest to compare the present exact

* For large Pr, the thermal boundary layer is much thinner than the velocity boundary layer. Correspondingly, $f \approx \eta$ and $f' \approx 1$ in equations (6) and (7). It then follows that θ and $\varphi\sqrt{(Pr)}$ are functions of $\eta\sqrt{(Pr)}$ alone.

solutions for uniform wall temperature with an approximate result derived by Erickson *et al.* from an energy integral. These authors derive the expression $Nu/\sqrt{(RePr)} = 0{\cdot}53$. This is seen to be in satisfactory agreement with the

Table 1. Heat-transfer results for laminar flow

Pr	$Nu/\sqrt{(RePr)}$ UWT	UHF
0·7	0·4174	0·7216
1·0	0·4438	0·7512
10	0·5314	0·8500
100	0·5545	0·8753

exact solutions in the range of high Prandtl numbers.

Lastly, it is also of interest to relate the present results with those of the Blasius problem. For instance, for $Pr = 0{\cdot}7$ and uniform wall temperature the respective values of $Nu/\sqrt{(Re)}$ are 0·349 and 0·293 for the continuous surface and the flat plate boundary layers. This same qualitative relationship applies for the entire Prandtl number range as well as for uniform wall heat flux. Thus, in common with the laminar friction coefficient the laminar heat-transfer coefficient for the continuous-surface boundary layer exceeds that for the flat-plate boundary layer.

Turbulent boundary layer

The turbulent velocity field is analyzed by applying the well established concepts of the law of the wall. The effects of the wake-like region at the edge of the boundary layer are not included in such an analysis. Measurements of turbulent velocity profiles, to be discussed later, suggest that the law of the wall provides a satisfactory representation across a substantial portion of the boundary layer now under consideration. The shear stress τ at any point in the flow is related to the local velocity gradient by means of the molecular viscosity μ and the eddy diffusivity for momentum ϵ_m

$$\tau = -(\mu + \rho\epsilon_m)\frac{du}{dy}. \tag{9}$$

It is convenient to employ the so-called universal velocity parameters u^+ and y^+

$$u^+ = u/\sqrt{(\tau_w/\rho)}, \qquad y^+ = y\sqrt{(\tau_w/\rho)}/\nu \tag{10}$$

in which τ_w is the local wall shear stress. By eliminating u and y in favor of u^+ and y^+ and additionally introducing

$$u^{++} = u_s^+ - u^+, \qquad u_s^+ = U_s/\sqrt{(\tau_w/\rho)} \tag{11}$$

one finds

$$\frac{\tau}{\tau_w} = \left(1 + \frac{\epsilon_m}{\nu}\right)\frac{du^{++}}{dy^+}. \tag{12}$$

Following Deissler [6], the flow field is subdivided into a region near the wall $0 \leqslant y^+ \leqslant y_1^+$ and a region away from the wall $y^+ \geqslant y_1^+$. In the former, $\tau/\tau_w \approx 1$; furthermore, by extending Deissler's model, one can write

$$\epsilon_m/\nu = n^2u^{++}y^+, \qquad n = 0{\cdot}109. \tag{13}$$

With these, equation (12) can be integrated in closed form

$$y^+ = \frac{1}{n}\sqrt{\left(\frac{\pi}{2}\right)}\exp\left[\tfrac{1}{2}(nu^{++})^2\right]\operatorname{erf}\left(\frac{nu^{++}}{\sqrt{2}}\right) \tag{14}$$

in which erf denotes the error function

$$\operatorname{erf}\psi = \frac{2}{\sqrt{\pi}}\int_0^{\psi}\exp(-\beta^2)\,d\beta. \tag{15}$$

Away from the immediate vicinity of the wall, it is well known that equation (12) integrates to a logarithmic velocity profile, i.e.

$$u^{++} = u_1^{++} + \frac{1}{\kappa}\ln\frac{y^+}{y_1^+}, \qquad y^+ \geqslant y_1^+. \tag{16}$$

A numerical value of 0·4 for κ is widely accepted in the literature. Furthermore, Deissler's studies have indicated that $u_1^{++} = 12{\cdot}9$ and $y_1^+ = 26$. With these, equation (16) becomes

$$u^{++} = 4{\cdot}75 + 2{\cdot}5\ln y^+, \qquad y^+ \geqslant y_1^+. \tag{17}$$

It may be noted that the velocity solution given by equations (14) and (16) is continuous at $y^+ = y_1^+ = 26$. It is interesting to observe that

the u^{++}, y^+ profile for the continuous-surface boundary layer is the same as the u^+, y^+ distribution for the flat-plate boundary layer. However, the u^+, y^+ profiles for the two problems are different, and this leads to differences in the friction coefficients as is later demonstrated.

With the velocity profiles now available, the friction coefficient may be determined from a momentum balance. Attention may be directed to a control volume spanning the boundary layer and contained between x and $(x + dx)$. The momentum principle states that the net outflow of momentum from the volume equals the net force. In mathematical terms, this is

$$\tau_w \, dx = d\left[\int_0^\delta \rho u^2 \, dy\right] \tag{18}$$

in which $y = \delta$ is the edge of the boundary layer. Upon noting that

$$dx = \frac{\nu}{u_s^+ \sqrt{(\tau_w/\rho)}} \, d(Re) \tag{19}$$

equation (18) may be rephrased as

$$d(Re) = u_s^{+2} \, d\left[\int_0^{\delta^+} \frac{(u_s^+ - u^{++})^2}{u_s^+} \, dy^+\right]. \tag{20}$$

The right-hand side of equation (20) can be integrated by parts, and from this there is obtained for the condition $\delta = 0$ at $x = 0$

$$Re = u_s^{+2} I(u_s^+) - 2 \int_0^{u_s^+} I(\tilde{u}_s^+) \, \tilde{u}_s^+ \, d\tilde{u}_s^+ \tag{21}$$

where $\tilde{u}_s^+$ is a dummy variable of integration and

$$I(\chi) = \int_0^\chi \frac{(\chi - u^{++})^2}{\chi} \frac{dy^+}{du^{++}} \, du^{++} \tag{22}$$

χ is also a dummy variable.

By employing the relationship between u^{++} and y^+ provided by equations (14) and (16), the variation of I with χ can be evaluated from equation (22). Then, returning to equation (21), the indicated integration may be performed. These operations were executed numerically. As an end result, one obtains the variation of Re as a function of u_s^+. However, from equations (4) and (11), which define c_f and u_s^+, there follows

$$c_f = 2/u_s^{+2}. \tag{23}$$

Thus, equation (21) provides the sought-for relationship between c_f and Re.

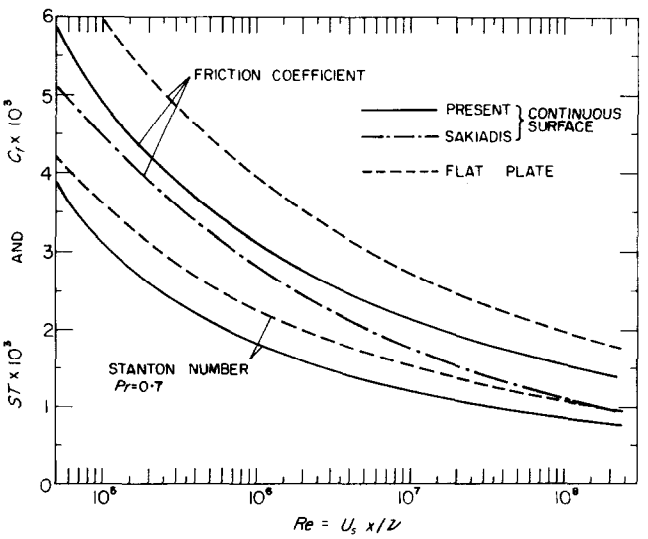

FIG. 3. Local friction coefficients and Stanton numbers for turbulent flow.

The local friction coefficient thus obtained is plotted as a solid line in the upper portion of Fig. 3. In accordance with prior boundary-layer results, c_f decreases with increasing Reynolds number. Also appearing in the figure is a dashed line representing the local friction coefficient for the flat plate; these results were derived by the authors following a procedure identical to that just outlined. It may be observed that the flat-plate results lie higher than those for the continuous surface. This is in contrast to the situation for the laminar boundary layer, wherein the friction coefficients for the continuous surface are greater than those for the flat plate.

Sakiadis' result for the continuous surface, derived by assuming a one-seventh power velocity profile, are shown in the figure as a dot–dashed curve. The latter falls from 10 to 25 per cent below the present results, depending on the Reynolds number. The one-seventh power law is widely recognized as being a gross approximation of the velocity field, whose utility diminishes at large Reynolds numbers.

The foregoing analysis is readily extended to yield average friction coefficients. In terms of of the drag force

$$D = \int_0^x \tau_w \, dx,$$

the average friction coefficient is defined as

$$\bar{c}_f = \frac{D/x}{\frac{1}{2}\rho U_s^2} = \frac{1}{x}\int_0^x c_f \, dx. \tag{24}$$

If one returns to the momentum balance, equation (21), and integrates both sides with respect to x, there can be derived

$$\bar{c}_f = \frac{2I(U_s^+)}{Re} \tag{25}$$

where I has already been defined in equation (22). As previously discussed, $I(U_s^+)$ is a unique function of the Reynolds number. Therefore, the relationship between $\bar{c}_f$ and Re is fully established as soon as the I integral is evaluated. These results are shown as a solid line in Fig. 4, which also contains curves for the flat plate and for Sakiadis' solution. The trends are the same as those already discussed in connection with the local friction coefficient.

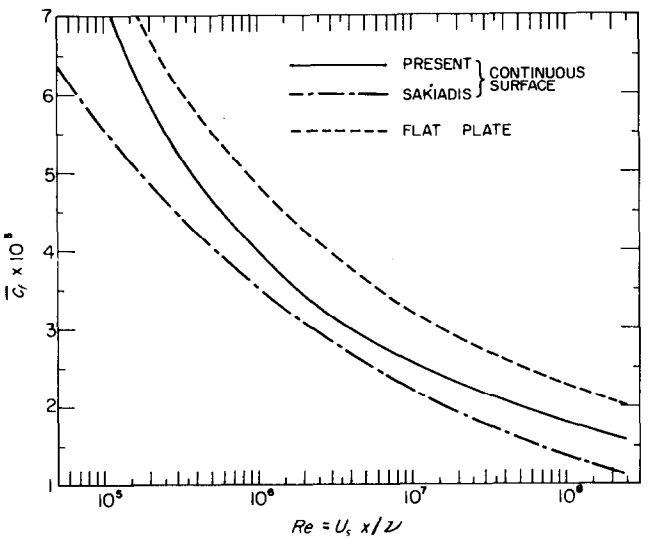

FIG. 4. Average friction coefficients for turbulent flow.

Consideration may now be given to the heat-transfer problem for the turbulent boundary layer. The analytical formulation closely parallels the foregoing velocity analysis. As a first step, the transverse heat flux q at any point in the flow is related to the local temperature gradient

$$q = -(k + \rho c_p \epsilon_h)\frac{dT}{dy}. \tag{26}$$

The first term in the parentheses is the molecular conductivity; while in the second term, ϵ_h is the eddy diffusivity for heat. It is now convenient to introduce a dimensionless temperature T^+

$$T^+ = \frac{(T_w - T)\rho c_p \sqrt{(\tau_w/\rho)}}{q_w}. \tag{27}$$

With this, and with the definition of y^+ from equation (10), the heat flux expression becomes

$$\frac{q}{q_w} = \left(\frac{1}{Pr} + \frac{\epsilon_h}{\nu}\right)\frac{dT^+}{dy^+}. \tag{28}$$

Experience with a wide range of external and internal turbulent flows has shown that the assumption of equal diffusivities for heat and momentum leads to heat-transfer predictions of acceptable accuracy, except for liquid metals. This assumption will also be invoked here.

In the region near the wall, $q/q_w \approx 1$ and $\tau/\tau_w \approx 1$. Then, upon comparing equations (28) and (12) and introducing $\epsilon_h = \epsilon_m$ from equation (13), there follows

$$dT^+ = \left[\frac{1 + n^2 u^{++} y^+}{(1/Pr) + n^2 u^{++} y^+}\right] du^{++}, \qquad 0 \leqslant y^+ \leqslant y_1^+. \tag{29}$$

When $Pr \neq 1$, this differential equation cannot be integrated in closed form and numerical means are required. However, this is not a major drawback since the evaluation of the heat-transfer coefficient, to be discussed later, also requires numerical integration.

For the region away from the wall, it is well established that $1/Pr \ll \epsilon_h/\nu$. Further, for Prandtl numbers that are not too different from unity, it may be assumed that $q/q_w \approx \tau/\tau_w$. With these simplifications, and with $\epsilon_m = \epsilon_h$, it follows that

$$dT^+ = du^{++}$$

or

$$T^+ - T_1^+ = u^{++} - u_1^{++}, \qquad y^+ \geqslant y_1^+. \tag{30}$$

The dimensionless temperature distribution can be evaluated from equations (29) and (30). These results will now be employed in determining the heat-transfer coefficient. From an energy balance on a control volume spanning the boundary layer and bounded by planes at x and at $(x + dx)$, there follows

$$q_w\, dx = d\left[\int_0^{\delta_h} \rho c_p (T - T_\infty)\, u\, dy\right] \tag{31}$$

where $y = \delta_h$ is the edge of the thermal boundary layer. Before proceeding, some decision must be made about the thermal boundary condition at the wall. For turbulent flow, it is known that the local heat-transfer coefficient is relatively insensitive to the nature of the thermal boundary condition. In particular, there is usually little difference between the results for uniform wall temperature and uniform heat flux. On the other hand, it can be demonstrated that the evaluation of the energy balance, equation (31), is very much more difficult for the uniform temperature condition than for the uniform heating condition. In light of the foregoing considerations, the analysis will be carried forward for the uniform heat flux case.

After introducing dimensionless variables in equation (31) and integrating with the condition $\delta_h = 0$ when $x = 0$, there results after rearrangement

$$T_\infty^+ = \frac{(Re/u_s^+) + \int_0^{u_s^+} (u_s^+ - u^{++})\, T^+ (dy^+/du^{++})\, du^{++}}{\int_0^{u_s^+} (u_s^+ - u^{++})(dy^+/du^{++})\, du^{++}} \tag{32}$$

From equations (14), (17), (29), and (30), it is evident that y^+ and T^+ are functions of u^{++}. Furthermore, it has been established previously that u_s^+ is a unique function of Re. The indicated integrations are performed numerically, and this yields a relationship between T_∞^+ and Re. Next, by making reference to equations (8) and (27), it can be verified that

$$T_\infty^+ = \left(\frac{\rho c_p U_s}{h}\right)\left(\frac{1}{u_s^+}\right). \tag{33}$$

The grouping $h/(\rho c_p U_s)$ is called the Stanton number and is denoted by St, so

$$St = \frac{h}{\rho c_p U_s} = \frac{1}{T_\infty^+ u_s^+}. \tag{34}$$

Since both T_∞^+ and u_s^+ are now known functions of the Reynolds number, so also is the Stanton number. The actual numerical calculations were performed for $Pr = 0{\cdot}7$, which is appropriate to gases. This choice was made with the experimental phase of the investigation in mind.

The Stanton number results thus derived are plotted as a solid line in the lower part of Fig. 3. A dashed curve is also shown which represents the results for the flat plate. In common with the turbulent friction coefficient, the Stanton number for the continuous surface is lower than that for the flat plate. This is just opposite to the heat-transfer results for the laminar boundary layer.

THE EXPERIMENTAL APPARATUS

Upon consideration of various design possibilities, a rotating drum system was selected to model the boundary layer on a continuous moving surface. As shown in the schematic diagram at the right of Fig. 1, the drum is fitted with a skimmer plate that fixes the origin of the boundary-layer flow. Provided that the radius of the drum is sufficiently large, curvature effects are negligible and the flow is essentially identical to that over a plane surface.

The details of the experimental apparatus are contained in Fig. 5, which is approximately to scale. The rotating drum is a right circular cylinder, 12·6 in. in diameter, 24 in. in length, and oriented with its axis vertical. The edge of the skimmer plate is in contact with the cylinder along its entire length. The skimmer is made of aluminium plate, 12-in wide and $\frac{1}{8}$-in thick. A piece of felt is glued to the edge of the skimmer to avoid metal-to-metal contact with the cylinder. The angular orientation of the skimmer with respect to the cylinder was adjusted to achieve separation-free flow in the region immediately downstream of the point of contact. Stationary annular plates are affixed at the upper and lower ends of the cylinder to inhibit axial inflow.

The cylinder itself was fabricated from mild steel piping (0·37-in wall thickness) that was carefully machined for concentricity. The outer surface was polished and buffed to a shiny finish that was protected with a thin film of oil when the apparatus was not in use.

The drum was heated to facilitate thermal measurements. Adjacent to the inner surface of the cylinder, and arranged longitudinally along it, are three identical but independent heaters. The top and bottom heaters are guards, while the intermediate heater serves the test section. The space between the inner wall of the cylinder and the shaft is filled with insulating material. Owing to the large heat capacity of the wall and to the high rotational speed, it is likely that the drum surface temperature was nearly circumferentially uniform.

The temperature of the cylinder wall is sensed by six thermistors strategically located so as to facilitate a balancing of the guard heater and test section temperatures. The thermistors are imbedded in the cylinder wall to within 0·050 in of the outer surface. The power supplied to the heaters and the signal from the thermistors are transmitted through slip rings located at the top of the cylinder-support shaft.

The use of thermistors instead of thermocouples for the wall temperature measurement was dictated by practical considerations relating to high-speed rotation. In order to insure high accuracy in the temperature measurements,

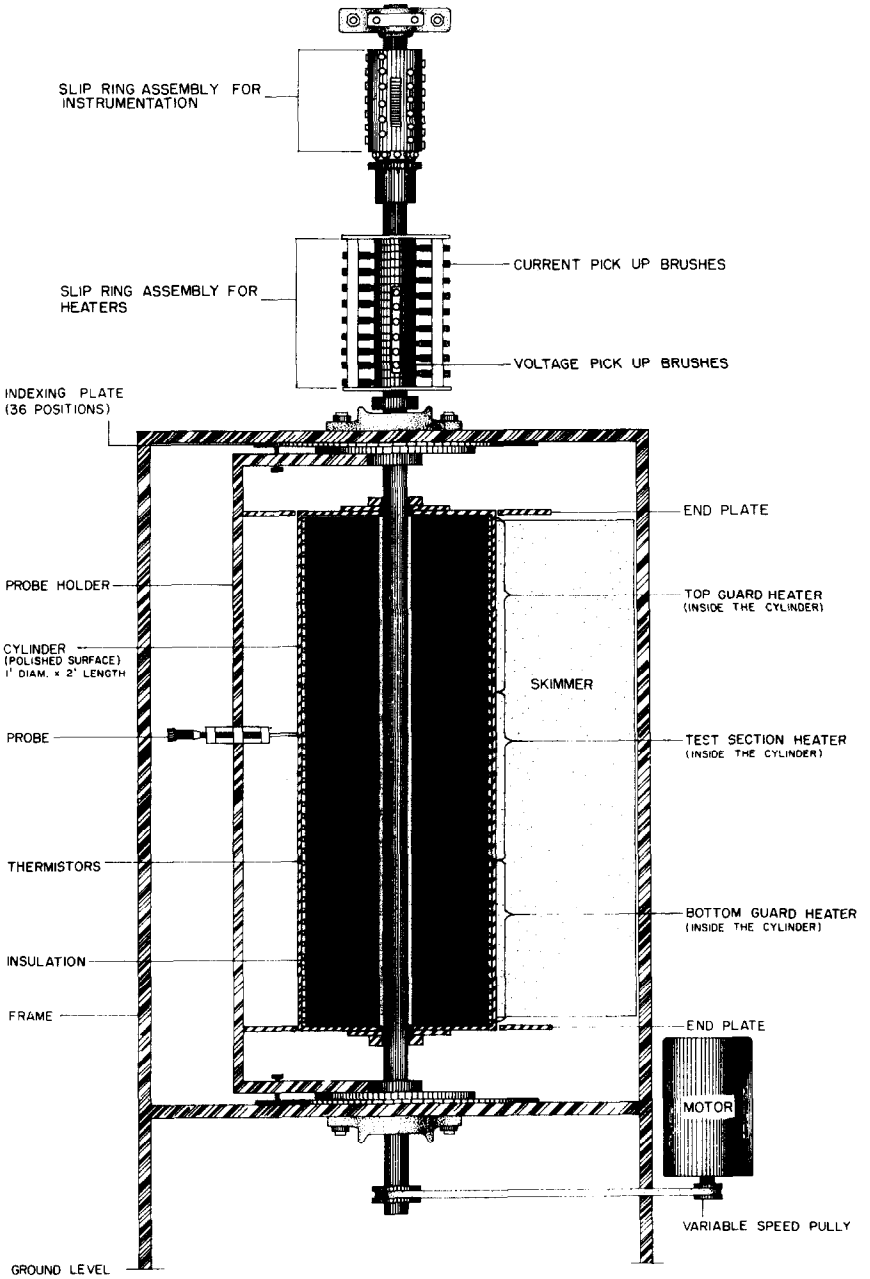

FIG. 5. Diagramatic representation of the experimental apparatus.

the thermistors were subjected to a systematic aging program that was preceded by and then followed by a careful calibration.

The drum was driven at rotational speeds ranging from 600 to 1500 rev/min by an induction motor through a variable-speed pulley. Prior to the execution of the experiments, a painstaking program of dynamic balancing and vertical alignment was carried out. At the conclusion of the adjustments, the rotating drum was remarkably quiet and vibration-free, particularly in view of its large size.

Either a velocity or a temperature probe may be mounted on a probe holder as shown in Fig. 5. Under normal operating conditions, the probe was situated in a horizontal plane mid-way along the length of the cylinder, although vertical movement is allowable.* The probe holder was designed to provide carefully controlled travel normal to the cylindrical surface at 10-degree intervals around the circumference. The 10-degree stop positions were fixed by indexing plates situated at the upper and lower ends of the cylinder. The various circumferential stations are identified as 1, 2, 3, ... n, corresponding to angular displacements of 10, 20, 30, ..., $10n$ degrees from the contact point of the skimmer. The radial travel was controlled by a micrometer head that could be read to within 0·005 mm.

Both the velocity and temperature probes were of small size in recognition of the small thickness of the boundary layer. The velocity probe was fabricated from stainless-steel hypodermic tubing whose tip was drawn and then flattened. The resultant impact opening is rectangular in shape, with dimensions 0·0027 × 0·0286 in. Measurements at probe Reynolds numbers below 30 were not made in cognizance of possible viscous errors [7–9]. The temperature probe is a thermocouple formed by 0·001-in chromel and constantan wires stretched between the arms of a supporting yoke and joined at the mid-span point. The thickness of the thermocouple junction is 0·0028 in. The temperature probe was carefully calibrated prior to use.

The impact pressure sensed by the velocity probe was read from a U-tube water manometer by a travelling microscope that can discriminate heights to within 0·0001 in. The output of the thermocouple probe was recorded by an integrating digital voltmeter with a calibrated accuracy of 3 mV. All other electrical quantities were measured with high-precision laboratory instruments. The rotational speed of the drum was determined from a revolution counter in conjunction with a stopwatch.

EXPERIMENTAL RESULTS

The laminar velocity field

The range of circumferential locations at which laminar flow existed was established by preliminary experiments employing both smoke tracers and a hot-wire anemometer. Subsequently, impact tube traverses were carried out at several circumferential stations at each of three rotational speeds. These velocity measurements have been brought together in Fig. 6, where they are plotted in terms of dimensionless. variables. The abscissa variable, $y\sqrt{(U_s/\nu x)}$, is the similarity variable that arises from the laminar boundary-layer analysis. The Reynolds number of the data ranges from 5×10^4 to $1{\cdot}5 \times 10^5$. The solid line that appears in the figure is the analytical solution.

In reducing the data, cognizance was taken of the possibility that the origin of the boundary layer need not necessarily coincide with the point at which the skimmer contacts the cylinder. To establish the effective origin of the boundary layer, a working graph was prepared on which were plotted the values of y^2 vs. x corresponding to a fixed value of $u/U_s = 0{\cdot}5$. According to laminar theory, such a plot should yield a straight-line relationship. The data verified this prediction. The point at which the aforementioned line crossed the abscissa axis was taken as the effective origin of the boundary layer.

* Preliminary tests verified that the velocity field was independent of vertical position, except very near the ends of the cylinder.

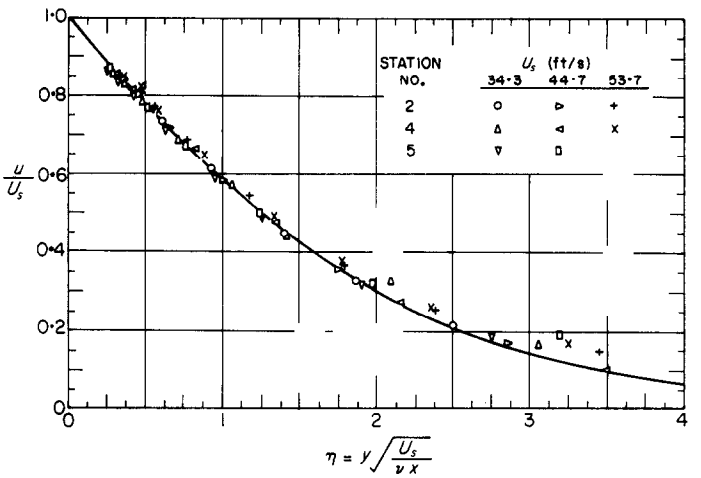

FIG. 6. Comparison of experimental and analytical laminar velocity profiles.

The effective origin differed only slightly for the three surface speeds (see p. 142 of reference [11]).

Inspection of Fig. 6 shows that not only are the data for the various conditions unified by the use of the similarity variable, but also, that there is very good agreement between theory and experiment. The data tend to fall slightly above the curve at large values of η; this is believed to be caused by disturbances in the room.

In the view of the authors, the special significance of the foregoing comparison is that it demonstrates the analytically describable boundary layer on a continuous moving surface is a physically realizable flow. Furthermore, it demonstrates that the present apparatus provides a workable means of producing such a flow.

The turbulent velocity field

To facilitate the turbulent flow measurements, it was deemed desirable to aid the establishment of a fully turbulent flow field. To this end, a trip wire, 0·006 in. in diameter, was installed parallel to the cylinder surface and 0·003 in from it. The trip was situated between the second and third stations of measurement, that is, between 20 and 30 degrees from the splitter plate. The region of fully turbulent flow was discerned by employing a hot-wire anemometer.

Fourteen turbulent velocity profiles at various circumferential stations and surface speeds were measured. The Reynolds-number range of the measurements extended from 10^5 to 6×10^5. A representative profile from among these is pictured in Fig. 7. The characteristics of this profile are typical of the turbulent boundary layer; namely, a sharp drop-off near the wall

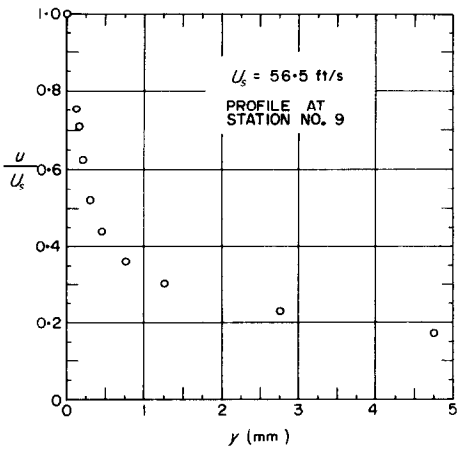

FIG. 7. Typical turbulent velocity profile.

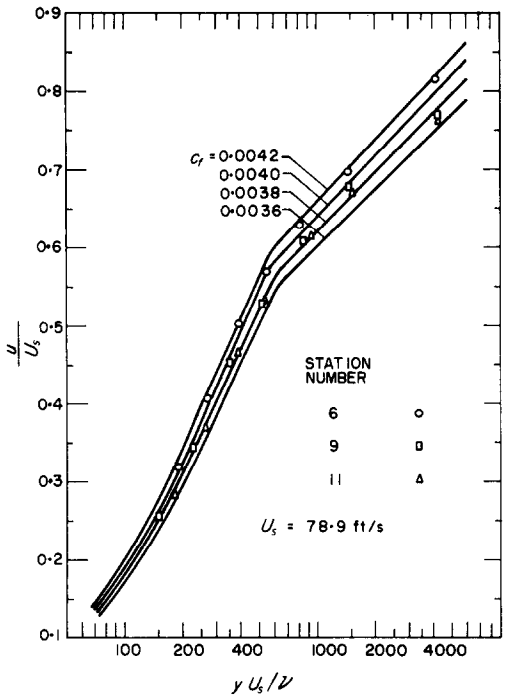

FIG. 8. Clauser-type plot for three representative turbulent velocity profiles.

and a subsequent gradual approach to the free stream condition.

After due consideration of the various possible approaches, it was decided to employ the Clauser-plot technique [10] to deduce friction coefficients from the measured velocity profiles. The basis of the Clauser plot is revealed by rephrasing the u^{++}, y^{+} variables from equations (10) and (11) as follows

$$u^{++} = \left(1 - \frac{u}{U_s}\right)\sqrt{\left(\frac{2}{c_f}\right)},$$

$$y^{+} = \frac{yU_s}{\nu}\sqrt{\left(\frac{c_f}{2}\right)}. \tag{35}$$

With a knowledge of the u^{++}, y^{+} distribution from equations (14) and (17), it is evident that one may plot curves of $1 - (u/U_s)$ vs. yU_s/ν for parametric values of c_f. The experimental data for each velocity profile can also be represented on a graph of $1 - (u/U_s)$ vs. yU_s/ν. The best fit of the plotted points to one of the analytical curves gives the value of c_f corresponding to the measured profile.

A representative Clauser plot for three of the measured velocity profiles is presented in Fig. 8. Since the distance between the successive stations is small, the difference in the corresponding Reynolds number is small and hence the difference in the friction factor must also be small. Among all fourteen runs, the experimental points fitted the curves quite well in the region near the wall; however, in some cases, the points are slightly below the curve in the region away from the wall.

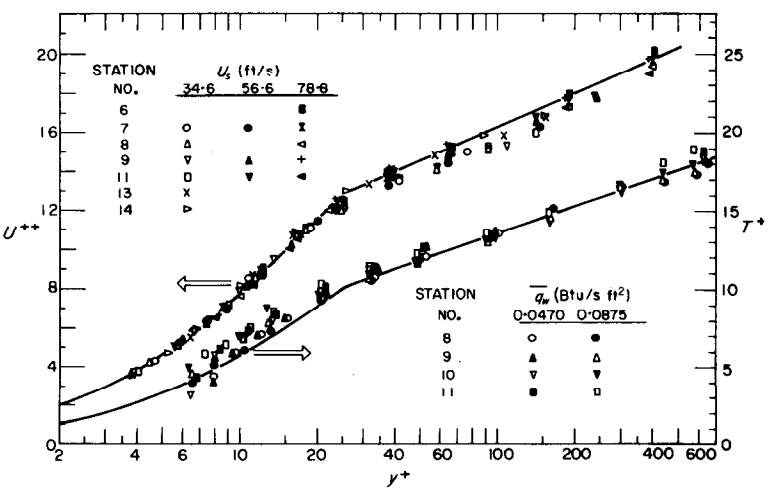

FIG. 9. Universal velocity and temperature profiles.

Once the c_f have been determined as described above, then the data for all profiles can be brought together on a universal u^{++}, y^+ plot as shown in the upper part of Fig. 9. The solid line represents the analytical solution. The data are in general accord with the analytical curve except for a few points at the larger y^+.

In order to permit a comparison between the experimental and the analytical results for the friction coefficient, it is necessary to determine the effective starting point of the boundary layer. The extrapolation is most conveniently carried out if use is made of the approximate relationship $c_f \sim Re^{-\frac{1}{5}}$. For a fixed value of U_s, one may plot c_f^{-5} vs. x. The abscissa intercept at which c_f^{-5} is zero provides the effective origin of the boundary layer.

The turbulent temperature field

Preliminary measurements revealed that, owing to its very small size and consequent small heat capacity, the thermocouple probe was extremely sensitive to temperature fluctuations. For example, the probe detected temperature variations on the order of 1 degF in the laboratory room. Substantially larger fluctuations were sensed in the thermal boundary layer.

It was deemed essential to reduce the boundary-layer temperature fluctuations before attempting to collect data. Two steps were taken to isolate the boundary layer from the room air currents. First, the entire apparatus was segregated from the remainder of the laboratory room by setting up a temporary plastic curtain around it. Next, a layer of copper screening was used to enclose the framework that supports the cylinder. The effect of these measures was to reduce the boundary-layer temperature fluctuations to half their original value.* In view of this, and with the additional proviso that data be collected only in the quiet hours after midnight, it was decided to proceed with the temperature measurements.

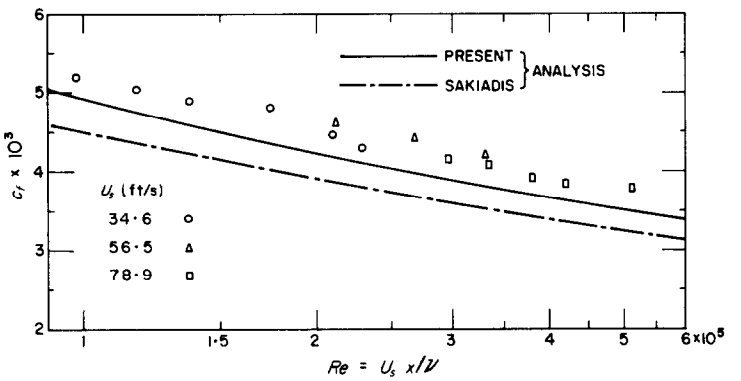

FIG. 10. Comparison of experimental and analytical turbulent friction coefficients.

Using the information from the Clauser plots and the just-determined x coordinates, one is able to display c_f as a function of the Reynolds number. These results are shown in Fig. 10 along with the theoretical predictions of the present investigation and those of Sakiadis. The measured values of c_f are about 6 per cent higher than the curve representing the present analysis. The good agreement between analysis and experiment can be taken as confirmation of the analytical model. The deviation of the data from Sakiadis' analysis is about 15 per cent.

* It was verified that the curtain and screening had practically no effect on the measured turbulent velocity profiles.

The continuing presence of the fluctuations, however, imposed certain limitations on the experimental procedure. First, measurements were performed only at the lowest rotational speed (about 600 rev/min). Second, owing to the fluctuations, standard hand-balance or self-balancing potentiometers were inadequate for detection of the thermocouple e.m.f. Instead, an integrating digital voltmeter was employed which integrated the input signal over a 1-s interval and printed the resultant millivolt reading on paper tape. For each fixed probe location, it was arranged that the meter would provide 25 of the aforementioned 1-s averages during a period of approximately 2 min. These 25 numbers were then punched on data cards and fed into a digital computer which was programmed to provide the average value and the standard deviation.

By following the procedure described above, profile measurements corresponding to turbulent flow conditions were performed at 4 circumferential stations at each of 2 heating rates. The respective wall-to-ambient temperature differences were approximately 60 degF and 30 degF. For the higher heating rate, at a typical probe location, the standard deviation of the 25 measurements from their average value was approximately 1 degF; at the lower heating rate, the corresponding standard deviation was about 0·5 degF. It is interesting to note that the boundary-layer temperature profiles extrapolated smoothly to the wall temperature as measured by the thermistors.

In consequence of the large heat capacity of the wall and the high rotational speed, it appears plausible to conclude that the thermal boundary condition corresponds closely to uniform wall temperature. Although the measurement of the power input to the test-section heater provides the circumferentially averaged wall heat flux, the local heat flux q_w must be otherwise determined. For this purpose, a graph analogous to the Clauser plot was constructed. The universal T^+ variable can be rearranged in the form

$$T^+ = [(T_w - T)\,\rho c_p U_s \sqrt{(c_f/2)}]/q_w. \qquad (36)$$

Since the T^+, y^+ distribution is available from the analysis, one can plot

$$[(T_w - T)\,\rho c_p U_s \sqrt{(c_f/2)}]$$

as a function of y^+ for parametric values of q_w. Furthermore, owing to the prior determination of c_f, the experimental temperature data can also be plotted in the same graph. The q_w which leads to the best correspondence between a given curve and the data is taken to be the local heat flux.

A representative plot of the type just described is shown in Fig. 11. The data correspond to station No. 8 (80 degrees from the contact point of the skimmer). As a matter of coincidence, the two values of q_w that parameterize

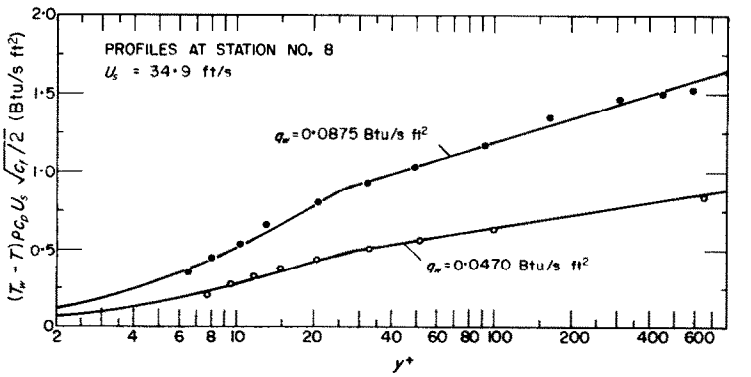

FIG. 11. Clauser-type plot for two representative turbulent temperature profiles.

the curves are identical to the measured average heat flux $\bar{q}_w$.

On physical grounds, one would expect that the heat flux at downstream locations be lower than that at station No. 8. Since the measurements were made only at stations 8, 9, 10, and 11, this decrease should be small (no more than 6 per cent according to theory). However, plots for the other stations analogous to Fig. 11 do not verify this trend. In fact, these plots indicate essentially no change in q_w.

To provide the most demanding test of the analytically predicted universal temperature profile, the T^+ values for the measurements at stations 9, 10 and 11 were formed using values of q_w deduced as follows: the q_w values in Fig. 11 were accepted as properly representing conditions at station 8, and the q_w at downstream stations were computed from these by applying the ratio of the corresponding local Stanton numbers from Fig. 3. This procedure should accentuate differences between the experimental and analytical T^+, y^+ distributions.

The experimentally determined T^+, y^+ distribution is shown in the lower part of Fig. 9, along with a solid line that represents the prediction of the analysis. Although the level of agreement is not as good as for the velocity field, it is, nevertheless, satisfactory. In appraising this comparison, it is well to recall that the analysis is for uniform wall heat flux, while the experimental conditions were, in all likelihood, closer to uniform wall temperature. On the other hand, turbulent temperature profiles are often relatively insensitive to the details of the thermal boundary condition.

The Reynolds-number range of the temperature measurements was too small to justify a graphical presentation of the Stanton-number results. Generally, the experimentally determined Stanton numbers fell below those of analysis. For instance, at $Re = 1{\cdot}1 \times 10^5$, the experimental and analytical values of Stanton number are 0·00265 and 0·00304 respectively. Part of this 13 per cent disparity might well be due to the fact that the analysis was performed for the case of uniform heat flux, while the experimental condition more closely approximated uniform wall temperature.

CONCLUDING REMARKS

On the basis of the laminar experiments and the excellent agreement of the measured profiles with theory, it may be concluded that an analytically describable boundary layer on a continuous moving surface is a physically realizable flow. Furthermore, the analytical model of the turbulent flow field is very well supported by the experimental data. The analytical predictions for the turbulent temperature field are in satisfactory agreement with the findings of experiment, but are not as well supported as are the results for the velocity field.

REFERENCES

1. B. C. SAKIADIS, Boundary-layer behavior on continuous solid surfaces: I. Boundary-layer equations for two-dimensional and axisymmetric flow, *A.I.Ch.E. Jl* **7**, 26 (1961).
2. B. C. SAKIADIS, Boundary-layer behavior on continuous solid surfaces: II. The boundary layer on a continuous flat surface, *A.I.Ch.E. Jl* **7**, 221 (1961).
3. B. C. SAKIADIS, Boundary-layer behavior on continuous solid surfaces: III. The boundary layer on a continuous cylindrical surface, *A.I.Ch.E. Jl* **7**, 467 (1961).
4. E. A. KOLDENHOF, Laminar boundary layer on continuous flat and cylindrical surfaces, *A.I.Ch.E. Jl* **9**, 411 (1963).
5. L. E. ERICKSON, L. T. FAN and L. C. CHA, The cooling of a moving continuous flat sheet, A.I.Ch.E. preprint No. 29, Eighth National Heat Transfer Conference, Los Angeles, California (August 1965).
6. R. G. DEISSLER and A. L. LOEFFLER, JR., Analysis of turbulent flow and heat transfer at high Mach numbers with fluid variable properties, NACA TN 4262 (1958).
7. C. W. HURD, K. P. CHESKY and A. H. SHAPIRO, Influence of viscous effects on impact tubes, *J. Appl. Mech.* **20**, 253 (1953).
8. F. A. MACMILLAN, Viscous effects on Pitot tubes at low speeds, *J. R. Aeronaut. Soc.* **58**, 570 (1954).
9. R. G. FOLSOM, Review of the Pitot tube, *Trans. Am. Soc. Mech. Engrs* **78**, 1447 (1956).
10. F. H. CLAUSER, Turbulent boundary layers in adverse pressure gradients, *J. Aeronaut. Sci.* **21**, 91 (1954).
11. F. K. TSOU, Velocity field, hydrodynamic stability, and heat transfer for boundary-layer flow along a continuous moving surface, Ph.D. Thesis, Department of Mechanical Engineering, University of Minnesota, Minneapolis, Minnesota (1965).

Résumé—Une étude théorique et expérimentale a été conduite sur l'écoulement et le champ de température dans la couche limite d'une surface en mouvement permanent. L'étude comprend à la fois les conditions d'écoulement laminaire et turbulent. Les solutions théoriques fournissent des résultats pour les distributions de vitesse et de température dans la couche limite et pour les coefficients de frottement et de convection. Les mesures du champ laminaire de vitesses sont en excellent accord avec les prévisions théoriques, vérifiant par là qu'une couche limite, descriptible mathématiquement, sur une surface en mouvement permanent est un écoulement réalisable physiquement. Les profils turbulents de vitesse déterminés par l'expérience sont aussi en très bon accord avec ceux de la théorie. On a trouvé un accord analogue pour les coefficients de frottement déduits des résultats expérimentaux par application de la technique du diagramme de Clauser. Les mesures des distributions de température, effectuées pour la couche limite turbulente, correspondent d'une façon satisfaisante avec la théorie.

Zusammenfassung—Eine kombinierte analytische und experimentelle Untersuchung der Strömung und der Temperaturfelder in der Grenzschicht einer kontinuierlich bewegten Oberfläche wurde durchgeführt. Die Untersuchung umfasst sowohl laminare als auch turbulente Strömungsbedingungen. Die analytischen Lösungen vermitteln Ergebnisse für die Grenzschichtgeschwindigkeit und Temperaturverteilungen, für Oberflächenreibung und Wärmeübergangskoeffizienten. Messungen eines laminaren Geschwindigkeitsfeldes stehen in sehr guter Übereinstimmung mit analytischen Voraussagen womit sie bestätigen, dass eine mathematisch beschreibbare Grenzschicht an einer kontinuierlich bewegten Oberfläche eine physikalisch realisierbare Strömung darstellt. Experimentell bestimmte turbulente Geschwindigkeitsprofile stimmen ebenfalls gut mit jener der Analyse überein. Ähnliche Übereinstimmung ergibt sich für Reibungskoeffizienten, die aus Messwerten auf Grund der Clauser-Aufzeichnungsmethode abgeleitet wurden. Messungen der Temperaturverteilungen in turbulenter Grenzschicht zeigen zufriedenstellende Übereinstimmung mit der Analyse.

Аннотация—Проведено одновременное теоретическое и экспериментальное исследование гидродинамики температурных полей в пограничном слое на непрерывно движущейся поверхности. Исследование включает как ламинарный так и турбулентный режим течения. Получены аналитические решения для скорости пограничного слоя и распределения температуры, коэффициентов поверхностного трения и теплообмена. Расчеты поля скорости ламинарного течения прекрасно согласуются с экспериментальными измерениями, что подтверждает физическую реальность математической модели пограничного слоя на непрерывно движущейся поверхности. Экспериментальные распределения турбулентной скорости также хорошо согласуются с теоретическими. Аналогичное соответствие найдено для коэффициентов поверхностного трения, обработанных графическим методом Клаузера. Измеренные распределения температуры в турбулентном пограничном слое удовлетворительно согласуются с теоретическими.